Journal of Applied Polymer Science

Interfacial Damage on Fatigue-Loaded Textile–Rubber Composites

Chloé Valantin,[1] Florian Lacroix,[1] Marie-Pierre Deffarges,[1] Julie Morcel,[2] Nourredine Aït Hocine[3]
[1]LMR, CERMEL, University of Tours, Joué-lès-Tours 37300, France
[2]Hutchinson, Joué-lès-Tours, France
[3]Laboratory of Mechanics and Rheology (LMR), CERMEL, INSA Centre Val de Loire, BP 3410 41034 Blois Cedex, France
Correspondence to: C. Valantin (E-mail: chloe.valantin@etu.univ-tours.fr)

ABSTRACT: To reach admissible lifetime expectancy, unidirectional textile–rubber composites must show a strong interface. Usually, it is achieved by coating the textile with Resorcinol–Formaldehyde–Latex (RFL). To evaluate fatigue impact on interfacial properties, composites with or without RFL are tested at different numbers of loading cycles and characterized through peel tests, dynamic mechanical analysis (DMA), scanning electron microscopy and energy-dispersive X-rays, and nanoindentation. For composites with RFL, the results indicate two main mechanisms for damaging: propagation of pre-existing fibrillar microcracks at the rubber/RFL interface completed by adhesive debondings at the RFL/textile interface. At first, the propagation of fibrillar microcracks is correlated with decrease of global composite peeling resistance and contribution of interphase to DMA damping. Then, RFL/textile debondings become critical. They are highlighted with a change of peeling failure surface and could be explained by RFL hardening, highlighted by nanoindentation. This questions the choice for RFL as a sustainable adhesive for composites under fatigue loading. © 2014 Wiley Periodicals, Inc. J. Appl. Polym. Sci. **2015**, *132*, 41346.

KEYWORDS: composites; degradation; elastomers; surfaces and interfaces; textiles

Received 25 May 2014; accepted 27 July 2014
DOI: 10.1002/app.41346

INTRODUCTION

For industrial goods such as tires, hoses, or belts, a strong interface between rubber and unidirectional continuous textile reinforcements (the cords) is needed to reach admissible power transmission and fatigue life. In this perspective, surface properties of the textile are usually enhanced with Resorcinol–Formaldehyde–Latex (RFL) through a dipping process as RFL biphasic structure favors textile adhesion with rubber. More precisely, RFL latex phase is expected to cocrosslink with rubber during the composite molding,[1,2] whereas its resorcinol–formaldehyde thermosetting resin phase is mainly aimed to provide textile bonding, thanks to its hydroxyl groups.

As it is an important aspect for fatigue life of textile or steel cord–rubber composites, many authors studied cord/rubber interfacial morphology and mechanical properties. Different approaches were used, from local observations to macroscopic characterizations.

Some researchers conducted static tests on specimens, as peeling,[3–5] or pulling out (*H*-tests[6–10] or *T*-tests [11–13]). They investigated on the impact of environmental conditions, rubber or adhesive formulations, and cord or rubber surface properties. However, such static measurements did not allow predicting interfacial strength behavior under fatigue loading. Therefore, specific geometries adapted to dynamic loading were developed.[14–19]

Another approach consisted in the application of fracture mechanics to study crack growth directly into cord–rubber composites.[20–22] To our knowledge, few authors carried out a deep investigation of interfacial damaging on single ply textile–rubber composite caused by tensile fatigue loading. One exception was Liu's experiment on unidirectional polyester cord–natural rubber (NR) composite. He pointed out three different fatigue damages: fiber–matrix debonding, matrix cracking, or cord break.[23]

A third way to study cord/rubber interfacial properties is to evaluate its width and/or its Young's modulus with nanoindentation or atomic force microscopy (AFM). Few researchers applied these techniques on cord–rubber composites. Wennekes[1] managed to measure local moduli on its aramid cord–NR composites with AFM. He highlighted an increase of average values when approaching RFL–rubber interface and attributed this to a local enrichment of rubber curatives. Using nanoindentation, Stevens plotted a moduli profile in a complex HNBR/adhesive/RFL/glass composite structure. So far, no study was carried out to follow the impact of fatigue loading on interfacial moduli.

A fourth way to evaluate interfacial adhesion on textile–rubber composites is to carry out a temperature sweep by dynamic mechanical analysis (DMA). Indeed, the decrease of matrix damping peak can highlight molecular motions of the matrix zone close to the fiber, called the "interphase." For example, when studying polyamide 6,6 reinforced SBR, Ibarra[25] observed a rubber damping peak decrease and an interphase damping peak appearance when a bonding system was added. To determine the energy dissipation at the interface owing to poor adhesion, tan δ_{int}, Zorowski and Murayama[26] introduced a model by subtracting experimental damping to a model one, corresponding to an ideal composite with perfect adhesion. When applying such model on polyamide 6,6 or PET cord–NR composite with different adhesives, Murayama correlated strong peeling strength with weak values of tan δ_{int}.[27] Excepting Afaghi-Khatibi's[28] experiments on carbon/epoxy composites, few investigations were done in terms of the impact of fatigue loading on DMA damping peak evolutions.

In this study, we propose to study polyamide cord–rubber composites submitted to severe fatigue loading. Under the test conditions applied, the main failure for composites with RFL-coated cords is a textile pull-out at the edges, assumed to be caused by interfacial weaknesses. Surprisingly, such failure is not observed when using uncoated cords. However, such composite without RFL cannot fulfill other industrial requirements.

Then, to explain fatigue damaging phenomena and RFL influence, we propose a multiscale and multitechnique approach with peel test, scanning electron microscopy and energy dispersive X-rays (SEM–EDX), nanoindentation, and DMA. Two types of composites, with or without RFL, are fatigue loaded at different times before characterization. The aim is to correlate interfacial evolutions, as microstructural damage or local moduli evolutions, to composite macroscopic mechanical properties, as peeling strength or damping.

EXPERIMENTAL

Material

The composite studied is made of a synthetic rubber matrix reinforced by continuous textile reinforcements.

Textile Structure

Textile reinforcements are made of continuous polyamide yarns made of microfilaments (diameter, ≈30 μm) twisted together to reach a diameter around 1 mm. Textiles are provided with and without RFL treatment, that is just before and after the last step of the dipping process. RFL coats the whole structure with a 2- to 20 μm thick layer.

Composites Elaboration

Continuous textile reinforcements, with or without RFL, are coated with a solvent-based rubber solution to get a good building tack. Then, they are stretched and placed in parallel between two rubber layers. The all-structure is vulcanized under pressure at 180°C for 15 min, driving to 1.7 mm thick composites (Figure 1).

Fatigue Loading of the Obtained Composites

Composites from the same batch, with or without RFL, are fatigue loaded on industrial test rigs at 100°C and 24 Hz, close to the conditions of use. Severe local tensile/compressive conditions are applied along the textile reinforcements' axe to accelerate textile/rubber damage by amplifying interfacial shear. The fatigue tests are stopped at different times (0.2, 2, 4, 6, 8, 14.5, 22, 29, 36, and 44 million cycles), all before the pull-out failure.

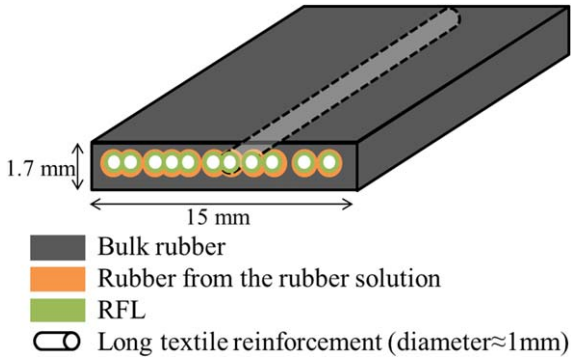

Figure 1. The textile/rubber composite with RFL. [Color figure can be viewed in the online issue, which is available at wileyonlinelibrary.com.]

Experimental Characterizations

180° Peeling Tests. Composites are cut inside the rubber with a razor blade, along the textile direction, through 15 mm. 180° peel test is carried out on an Alpha Technology T2000 at 50 mm/min, on such cracked initiated composites following ASTM D413.

Scanning Electron Microscopy and Energy-Dispersive X-rays. SEM–EDX observations intend to precisely locate peeling breakings and quantify fatigue damages on transversal cuts of the composites.

Previously, EDX analyses of rubber sheets or RFL-coated textile have been used as references. They allowed the identification of atomic tracers: potassium and sodium for the RFL and zinc, chlorine and silicon for the rubber.

Composite cuts are made perpendicularly to the textile reinforcements' axe with razor blades. Obtained surfaces and peeled ones are sputter coated in a vacuum evaporator, with platinum for pictures and carbon for EDX analyses. A Zeiss ULTRA Plus or a JEOL JSM-6480LV equipped with an Energy-Dispersive System PGT Sahara detector is used.

Nanoindentation. Nanoindentation is carried out on cut specimens using a NanoTest Vantage from Micro Material, employing a Berkovich tip (Figure 2). Each indent is characterized by a loading, dwelling, and unloading phase. The maximum load, which remains constant during the dwelling phase, was set to 1 mN. Loading and unloading rates are ± 0.01 mN s^{-1}. To dissipate viscous effects, a holding time is used at maximum load: 300 s for accurate elastic modulus measurements and 60 s for moduli profiles. To precisely locate the indents on the different composite materials, an optical microscope is used.

For the determination of the indentation modulus, the Oliver and Pharr method is used.[29] Then, the indentation modulus or reduced modulus E_r is determined by:

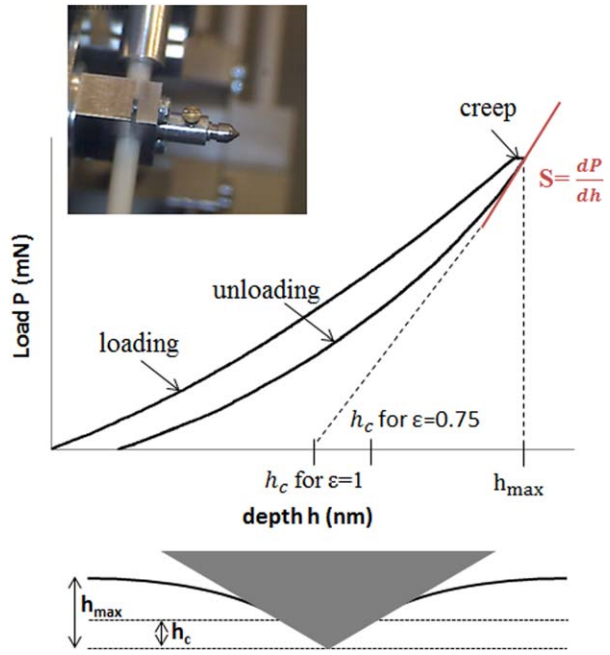

Figure 2. Diamond Berkovich tip used and nanoindentation curve example with graphical interpretation of the contact depth h_c. [Color figure can be viewed in the online issue, which is available at wileyonlinelibrary.com.]

$$E_r = \frac{S\sqrt{\pi}}{2\sqrt{A_c}} \quad (1)$$

where $S = dP/dh$ is the initial slope of the unloading curve (software calculated), P the applied force, and A_c the projected contact area of the tip at the contact depth h_c (Figure 2).

For a perfect indenter on a material not involving pile-up as it is the case in this study:

$$A_c = 3\sqrt{3}\tan^2 65.3 h_c^2 = 24.56 h_c^2 \quad (2)$$

$$h_c = h_{max} - \varepsilon \frac{P_{max}}{S} \quad (3)$$

with ε being a dimensionless geometric parameter (0.75 for a Berkovich tip).[30]

Young's modulus E can then be determined from

$$\frac{1}{E_r} = \frac{1-\nu^2}{E} + \frac{1-\nu_i^2}{E_i} \quad (4)$$

where ν is Poisson's ratio of the tested material and ν_i, E_i are Poisson's ratio and Young's modulus of the indenter (0.07 and 1140 GPa for the diamond tip used here).

Dynamic Mechanical Analysis. Composites (30 mm × 15 mm × 1.7 mm) are tested along the textile direction using a Metravib VA4000 in a temperature range from −100 to +250°C, at a frequency of 30 Hz, a strain of 0.3% and a heating rate of 3°C/min. Textiles are characterized by following the same procedure. Glass transitions $(T_g)_{30\ Hz}$ are taken at the maximum value of the damping term, tan δ.

RESULTS AND DISCUSSIONS

Interface Strength Investigated by 180° Peel Tests and SEM–EDX

First, to follow fatigue damages, 180° peel test is carried out on the two types of composites (with or without RFL). With a minimum of two tests per fatigue time, peel strength is plotted versus number of cycles (Figure 3) and failure surfaces are observed through optical microscopy and SEM–EDX.

For the composites with RFL, peel strength is divided by three after 44 million of fatigue loading cycles, which could indicate interface weakening. A logarithmic decrease is observed until 15 million cycles and it is followed by a linear decrease just after a small jump in the peel strength values. This graphic singularity defines what we propose to call the "transition zone" that we will deeper investigate in further experiments.

Optical observations of the composite failure surfaces correlate this singularity with a change of failure surface [Figure 4(a)]. Indeed, for composites with RFL, before fatigue loading, peeling front crack appears to propagate in a thin layer of rubber at the top of the RFL-coated textile. The location of the failure is confirmed by silicon and zinc EDX detections, the characteristic atoms of rubbers' formulations, at both sides of the peeled surfaces [Figure 5(a)]. Such cohesive failure inside an interfacial rubber layer, instead of a pure adhesive failure, could indicate that some interpenetrations and/or chemical bonds have been developed between RFL and rubber during composite molding.

Above 15 million cycles, peeling failure surfaces show sporadic polyamide delamination areas [Figure 4(a)] where iodine is detected by EDX [Figure 5(b)]. Indeed, this atom is the characteristic of the greige textile surface and potentially comes from heat stabilizers added into the polyamide formulation.[31] Between 15 and 44 million cycles, the total area of such RFL/textile delamination significantly increases and drives to almost 100% of adhesive breaking [Figure 4(a)]. Then, the peeling strength singularity around 15 million cycles Figure 3 could highlight a change of weak layer, corresponding to a peeling crack tip displacement from a thin rubber layer above the RFL/rubber interface, to the RFL/textile interface. Such final adhesive failure questions the strength and durability in fatigue loading of RFL/textile bonds.

Interestingly, for composites without RFL, the peeling strength values are few influenced by fatigue loading (Figure 3) and the failure surfaces almost show the same total area of adhesive

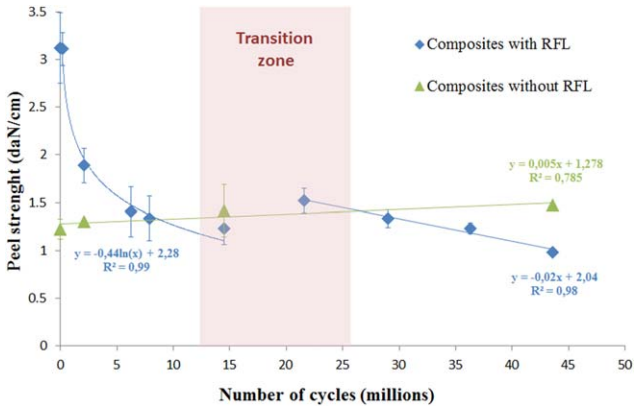

Figure 3. Peel strength evolutions with fatigue. [Color figure can be viewed in the online issue, which is available at wileyonlinelibrary.com.]

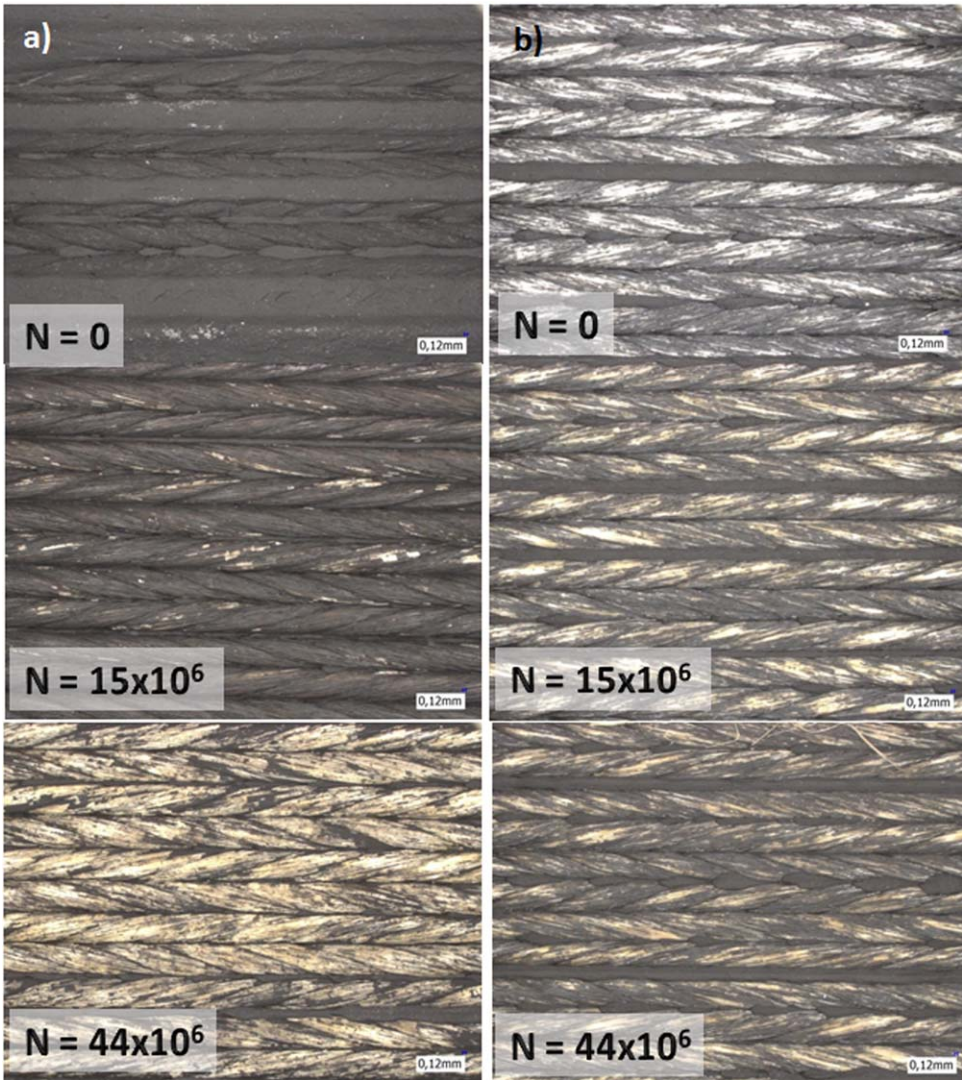

Figure 4. Optical views of failure surfaces after peeling tests on composites fatigue loaded for different number of cycles *N*. (a) With RFL and (b) without RFL. [Color figure can be viewed in the online issue, which is available at wileyonlinelibrary.com.]

fibers/rubber delamination regardless of fatigue time [Figure 4(b)].

To sum up, comparing the two types of composites, RFL appears to enhance rubber/textile static adhesion at the initial stage, driving to peeling strength values three times higher. However, after fatigue loading, such improvement is not kept. The logarithmic decrease of peel strength values until 15 million cycles could then indicate damages at the RFL/rubber interface and the following change of peeling failure surface is assumed to highlight another degradation phenomenon, located at the RFL/textile interface.

To validate this hypothesis and link macroscopic peeling tests results to microstructural evolutions, SEM observations are carried out on transversal cuts of the composites.

Fatigue Damages Followed by SEM–EDX on Transversal Cut Composite with RFL. For composites with RFL, at least two transversal cuts, containing an average of 12 textile sections, are analyzed at different fatigue times from 0 to 44 million cycles.

SEM observations reveal two types of textile/rubber fatigue damages:

1. Fibrillar microcracks at the RFL/rubber interface [Figure 6(a)].
2. Adhesive debondings between RFL and polyamide microfibers [Figure 6(b)].

RFL/rubber fibrillar microcracks. On each side of such microcrack, atomic compositions are clearly different (Figure 7). On one side [Figure 7(a)], EDX spectrum is the characteristic of the RFL layer and reveals potassium, potentially coming from latex stabilizers or potassium hydroxide used for pH adjustments during RFL formulation steps.[1,2] It was not the case for RFL coated-textile but zinc is detected, revealing chemical diffusions from the rubber into the RFL during composite molding. On the other side of the microcrack [Figure 7(b)], silicon, the characteristic atom of the rubber formulation, is strongly detected.

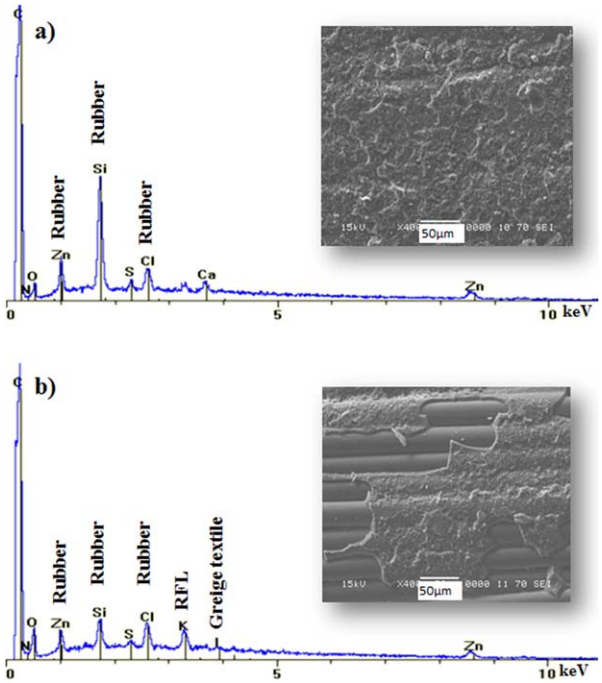

Figure 5. SEM–EDX of peeling failure surfaces of composites with RFL for (a) 0 and (b) 44 million cycles of fatigue loading. [Color figure can be viewed in the online issue, which is available at wileyonlinelibrary.com.]

Interestingly, fibrils till 2 µm long and 50 nm thin are observed inside the cracks, on the rubber side, regardless of fatigue time (Figure 8). Such fibrillation process is expected to absorb fracture energy driving to a decrease of the propagation speed of RFL/rubber cracks during fatigue loading.[32] It could be the evidence of interactions between RFL and rubber after molding, as chemical anchoring, covalent bonding or Van der Walls interactions, and could explain the reason why the previous peeling failure surface never showed a neat RFL surface but always rubber residues.

The second time, a method is developed to follow the microcrack propagation with fatigue. For this purpose, the RFL/rubber delamination $D_{RFL/rubber}$ is defined as:

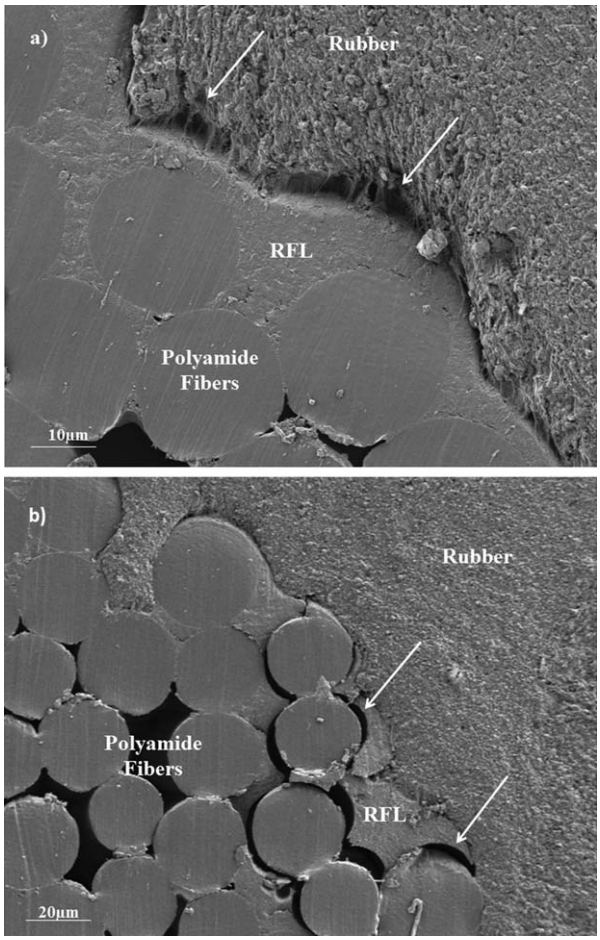

Figure 6. SEM images of (a) RFL/rubber microcracks and (b) RFL/fiber adhesive debondings.

$$D_{\mathrm{Rfl/rubber}(\%)} = \frac{\sum_{\text{textile 1}}^{\text{textile } N} \text{Microcracks length per textile}}{\sum_{\text{textile 1}}^{\text{textile } N} \text{Interfacial length between RFL and rubber}} \times 100 \quad (5)$$

where N is the number of textile reinforcements in the composite.

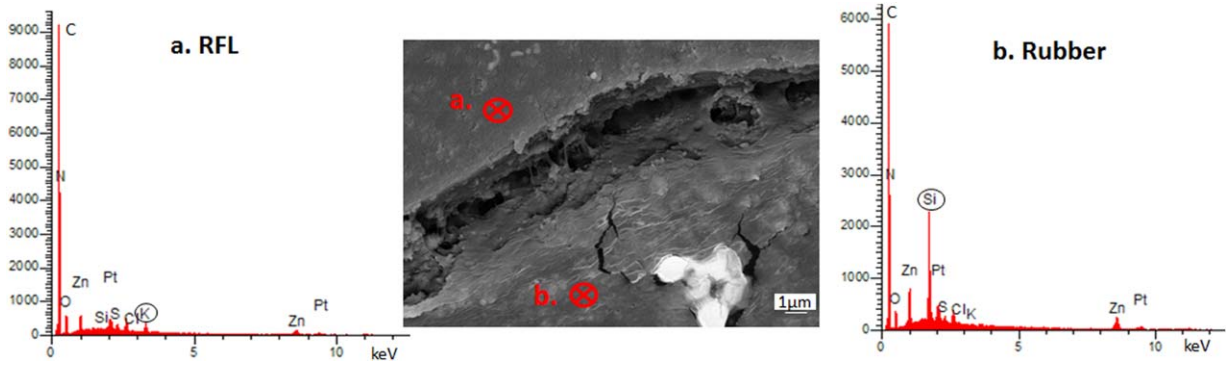

Figure 7. EDX spectra on each side of the RFL/rubber interface before fatigue loading. [Color figure can be viewed in the online issue, which is available at wileyonlinelibrary.com.]

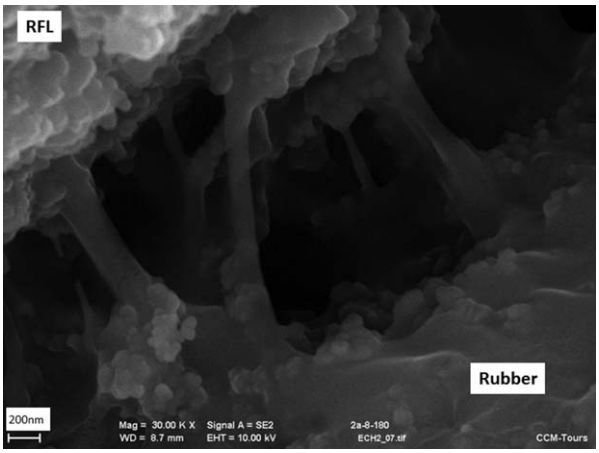

Figure 8. SEM image of the fibrillar structure of one RFL/rubber microcrack.

For each fatigue time, a minimum of two transversal cuts are observed by SEM. The measurements are then carried out on ~24 textile reinforcements and plotted in Figure 9. The average number of microcracks per textile reinforcement is also calculated and then the average microcrack length. All resulted data are shown in Figure 10.

Even before fatigue loading, thin RFL/rubber microcracks are detected and cover ≈20% of the total interface length (Figure 9). For each textile reinforcement, an average of ~30 cracks of 15 ± 2 μm long are pointed out (Figure 10).

Partially caused by the transversal cut, those cracks, nevertheless, highlight a weakness at the RFL/rubber interface. Regarding material properties and process parameters, such initial damages could have many origins, incriminating, for example, rubber/RFL wetting, diffusion, and cocuring or textile relaxation during composite molding.

After 44 millions of fatigue cycles, around 60% of the RFL/rubber interface is damaged (Figure 9). Looking closer, such interfacial delamination seems to evolve in three stages. The first lasts 8 million cycles and is correlated with a small increase of cracks thicknesses. The second stage is slower and correlated with the peeling strength transition zone previously introduced. A third faster stage is highlighted just before textile pull out.

Concerning microcrack average lengths (Figure 10), they reach 40 μm at 44 million cycles. However, microcracks remain almost as numerous as the beginning (≈30 per textile). As a result, interfacial delamination between RFL and rubber seems to be mainly caused by the propagation of pre-existing cracks than by a nucleation phenomenon.

RFL/polyamide microfiber debondings. In contrast to RFL/rubber cracks, RFL/polyamide fiber debondings do not show any fibrils [Figure 6(b)]. To study their evolution with fatigue loading, the fiber/RFL debonding content $D'_{\mathrm{RFL/fiber}}$ is defined as:

$$D_{\mathrm{RFl/rubber}(\%)} = \frac{\sum_{\text{textile 1}}^{\text{textile } N} \text{Number of debonded microfilaments}}{\sum_{\text{textile 1}}^{\text{textile } N} \text{Total number of microfilaments in contact with the RFL layer}} \times 100 \quad (6)$$

where N is the number of textile reinforcements in the composite.

As shown in Figure 11, this ratio shows a global increase, especially above the "peeling transition zone."

Such RFL/fiber debonding could contribute to the textile pull-out fatigue failure mode investigated here. Indeed, it echoes the failure surface change above 15 million cycles, highlighted by the previous peeling tests. It is also interesting to notice that only 22% of RFL/fiber debondings at 44 million cycles are correlated with almost 100% of such delamination on peeling failure surface. This evidences that peeling surface failures are sensitive to interfacial damage but cannot be directly linked with microcrack length measurements.

RFL/fiber debonding could also explain the decrease of RFL/rubber microcrack propagation speed in Stage 2 (Figure 9), consuming part of the mechanical energy given to the system.

Fatigue Damages on the Composites Without RFL

Rubber/textile cracking is not observed in initial composites without RFL [Figure 12(a)]. This could be partly explained by a better mechanical anchorage of the rubber on the textile because of its higher roughness. Surprisingly, even if the interface morphology appears more degraded, cracks are still not observed after fatigue loading [Figure 12(b)].

These results validate the fact that rubber/RFL or rubber/textile interfacial delamination is a propagation phenomenon of pre-existing cracks. It also clearly incriminates the role of RFL layer property evolutions in the damaging mechanism.

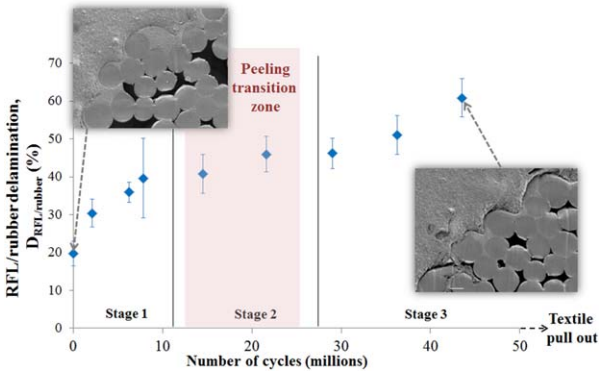

Figure 9. RFL/rubber interfacial delamination versus fatigue loading. [Color figure can be viewed in the online issue, which is available at wileyonlinelibrary.com.]

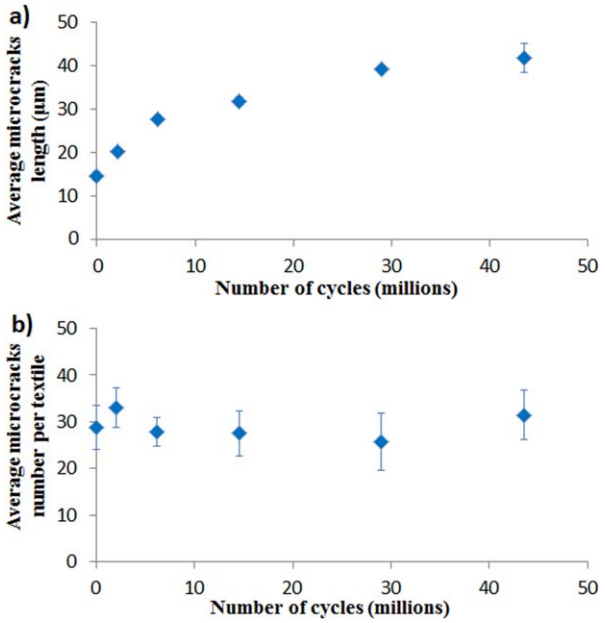

Figure 10. Average RFL/rubber microcracks (a) length and (b) number per textile versus fatigue loading. [Color figure can be viewed in the online issue, which is available at wileyonlinelibrary.com.]

With the aim to explain the differences between the two types of composite, interfacial moduli variations, with distance from the interface to fatigue loading time, are compared.

Local Mechanical Evolutions Characterized by Nanoindentation

Composites with RFL. A minimum of 10 indentation experiments are carried out in the following materials: polyamide fibers, RFL, "interfacial material" (in the rubber, 2 µm from the RFL/rubber interface), and bulk rubber (30 µm from the interface).

Examples of nanoindentation curves after different fatigue loading times are shown in Figure 13. With steeper unloaded slopes and narrower creep plateau, curves indicate a hardening and a decreasing ability to flow for both fatigue-loaded RFL and bulk rubber material.

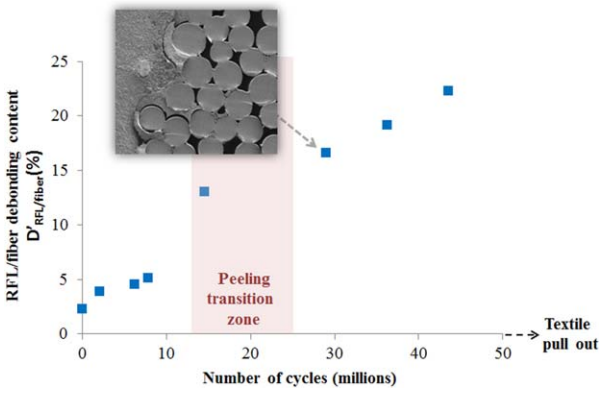

Figure 11. RFL/fiber debondings content versus fatigue loading. [Color figure can be viewed in the online issue, which is available at wileyonlinelibrary.com.]

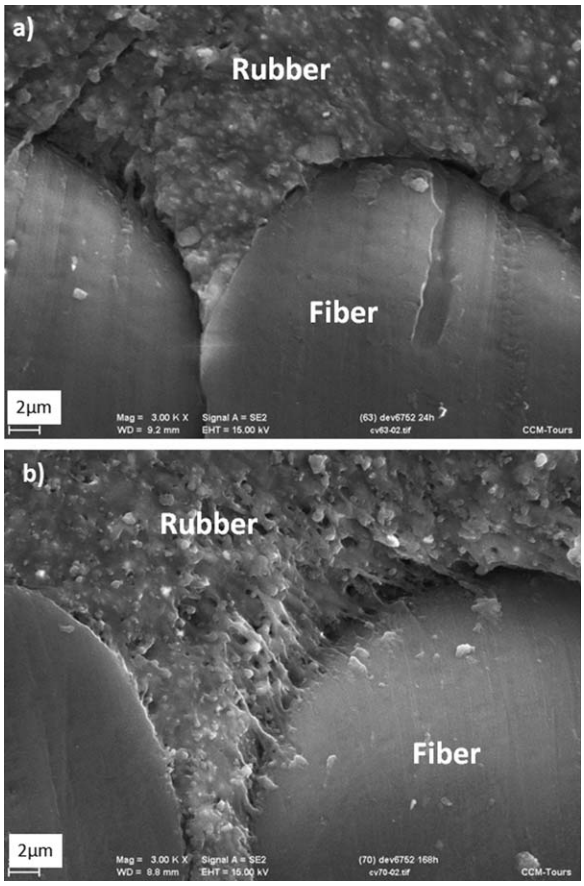

Figure 12. Rubber/textile interface on composites without RFL (a) before and (b) after 15 million cycles of fatigue loading.

For each curve, the indentation modulus E_r is calculated from eq. (1) and the values are averaged for each material and fatigue time. When observing evolutions (Figure 14), the rather stability of polyamide values from 3.2 to 4.2 GPa are first noticed. Concerning bulk rubber (i.e., far from the interface), a small increase is pointed out from 48 to 170 MPa.

Taking $\nu_{rubber} = 0.5$ and $\nu_{PA} = 0.4$ from the literature, the corresponding Young's modulus is calculated from eq. (4). Initial values for the polyamide ($E_{PA} = 2.7$ GPa) and the rubber ($E_{rubber} = 40$ MPa) are in the expected order of magnitude for such materials.

RFL and interfacial material moduli evolutions with fatigue are more significant (Figure 14).

Concerning the RFL, its indentation modulus starts from 1.5 GPa, corresponding to a Young's modulus of 1.2 GPa (taking $\nu_{RFL} = 0.45$). This value is close to the ones reported by Stevens of 1–1.5 GPa for the RFL inside its HNBR/adhesive/RFL/glass composite.[24] Nevertheless, using AFM, Wennekes pointed out RFL Young's moduli of 25–60 MPa on its aramid cord–NR composites.[1] The values measured in this study by nanoindentation are then more than 20 times higher. This fact could be explained by viscoelastic creep effects[33,34] or an underestimation of the contact area, as attractive forces between the RFL and the diamond Berkovich tip are neglected here.[29,35,36] It could also

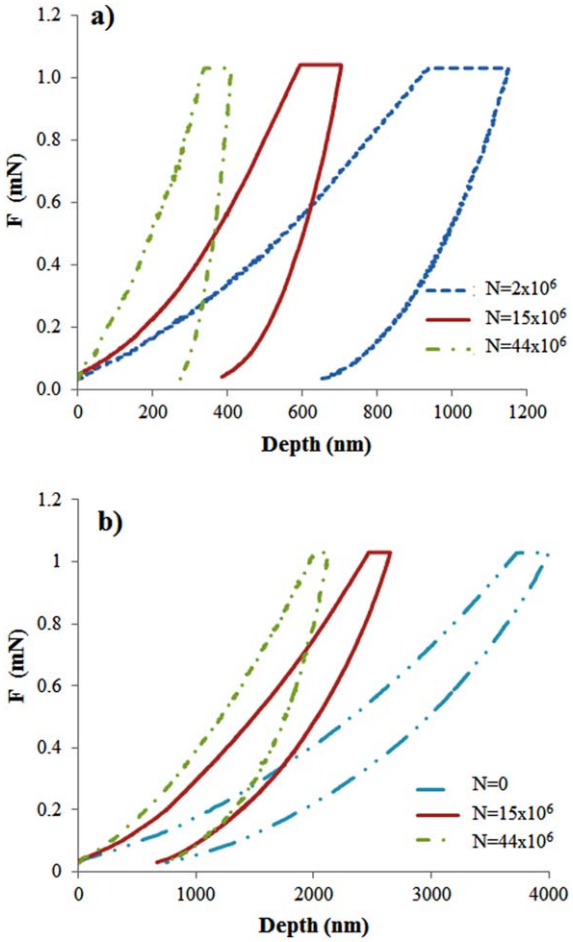

Figure 13. Indentation curves at different fatigue loading times for (a) RFL and (b) bulk rubber (holding time = 300 s). [Color figure can be viewed in the online issue, which is available at wileyonlinelibrary.com.]

be explained by the different RFL formulations investigated here and/or chemical diffusions from rubber to RFL, occurring during molding. For example, EDX analysis carried out on a transversal cut of the composite before fatigue loading revealed zinc inside the RFL layer, whereas this atom was not detected on RFL-coated textile (Figure 7).

After 44 million cycles, Young's modulus of the RFL reaches 5 GPa. Such RFL hardening needs to be further studied, but it could be attributed to a thermal embrittlement of resorcinol–formaldehyde resin network and/or chemical diffusions favored by the fatigue loading performed at 100°C.

Concerning the interfacial material, that is the rubber close to the interface, a Young's modulus of 350 MPa is measured before fatigue loading. This value is nine times higher than bulk rubber. Wennekes[1] and Stevens[24] highlighted an increase of rubber modulus when approaching the rubber/reinforcement interface. Wennekes attributed this to an interfacial enrichment in rubber curatives.

After fatigue loading, a strong modulus increase is also highlighted for the interfacial rubber. In fact, the $E_{\text{interfacial material}}/E_{\text{RFL}}$ ratio starts around 0.3 and reaches 1 after 44 million cycles, meaning that the RFL/rubber interface is becoming more and more homogeneous in terms of modulus. This phenomenon could be explained by a network densification and/or chemical interdiffusions with the both favored by a local heat generation owing to interfacial shearing.

Regarding the first explanation, it is worth noticing that studying PMMA/elastomeric joints being covulcanized at different temperature, Wootthikanokkhan et al.[37] pointed out that a highly crosslinked elastomer was correlated with a low peeling strength of the joint. They found a linear relationship between the peeling strength and the molecular weight between crosslinks, M_c. Such phenomenon could be explained by Lake and Thomas theory on crack growth in elastomers.[38] Considering that the plane of crack propagation is crossed by polymer chains whose crosslinks lie on opposite side, higher crosslink density reduces the number of bonds between crosslinks to be stressed to break one. Then, for fatigue-loaded cord–rubber composite, assuming that $E_r = f(1/M_c)$, the drop of peeling strength before 20 million cycles, that is when the failure is happening inside an interfacial rubber layer, could be correlated with the hardening of such layer, caused by an increase in crosslink density.

Regardless of the level of network densification or chemical interdiffusions being involved, modulus homogenizing between interfacial rubber and RFL leads to an interfacial area less sensitive to stress singularity. This could explain the reason why RFL/rubber interfacial delamination speed decreases in the second stage of fatigue loading as observed by SEM (Figure 9). This is for the benefit of another damaging phenomenon: RFL/fiber debondings.

To better visualize indentation modulus gradient through RFL/rubber interface, profiling is carried out on composite with or without RFL, before fatigue loading and after 44 million cycles (Figure 15).

Indentation Moduli Profiles. *Composites with RFL.* Before fatigue loading [Figure 15(a)], rubber indentation moduli increase until the rubber/textile interface, which is consistent

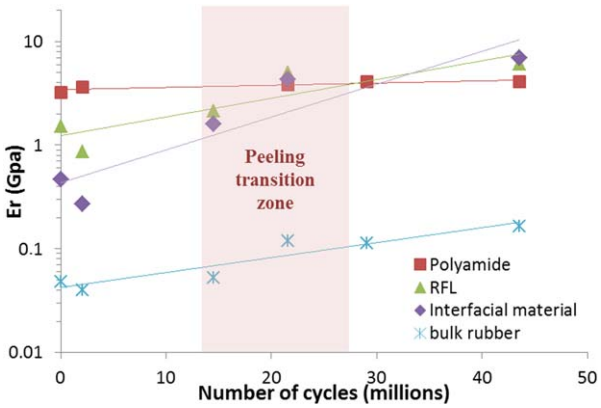

Figure 14. Average indentation moduli versus fatigue loading for each material of the composite with RFL (holding time = 300 s). [Color figure can be viewed in the online issue, which is available at wileyonlinelibrary.com.]

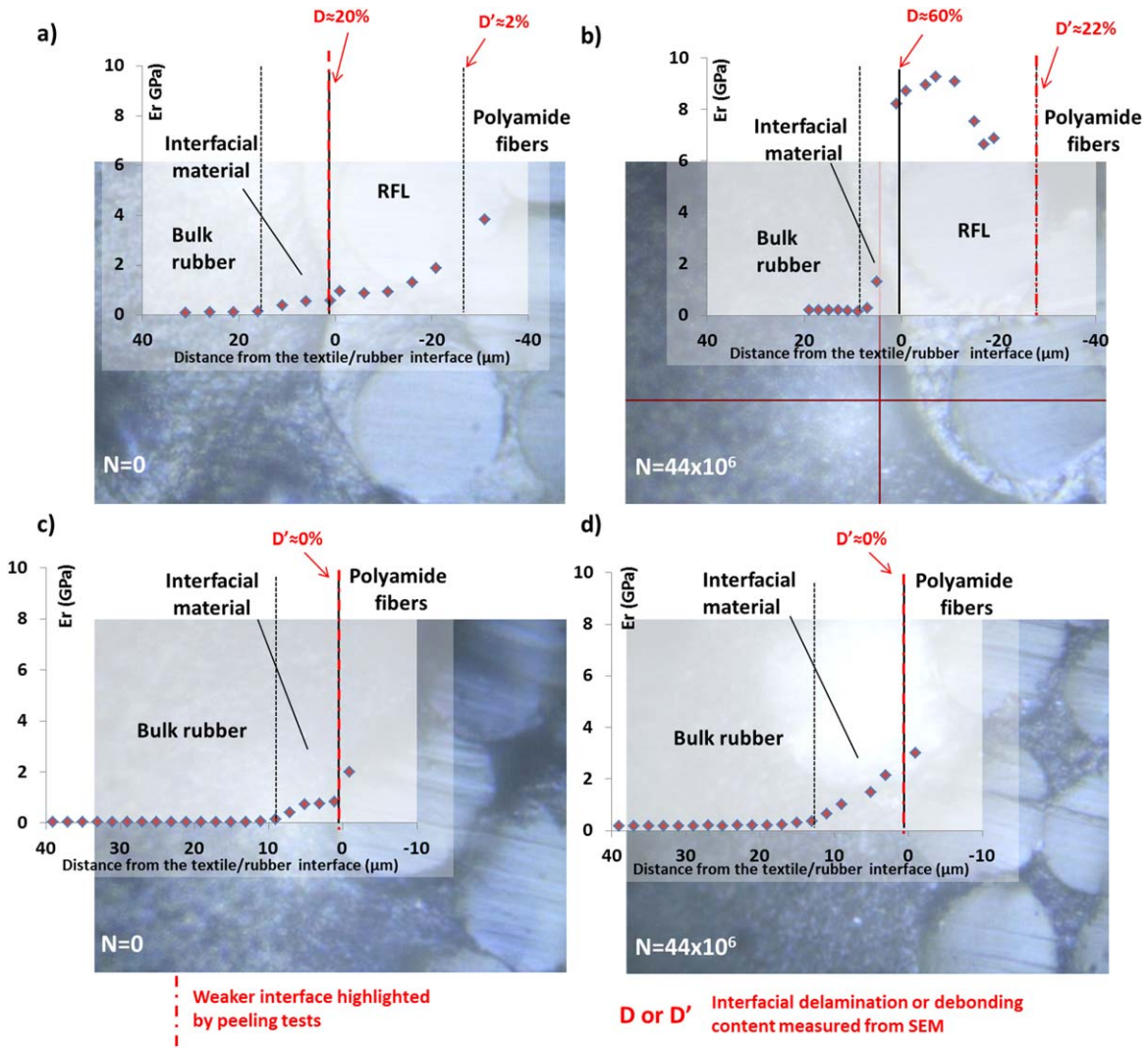

Figure 15. Indentation modulus across the textile/rubber interface on composites before and after 44 million cycles of fatigue loading (a, b) with RFL and (c, d) without RFL (holding time = 60 s). [Color figure can be viewed in the online issue, which is available at wileyonlinelibrary.com.]

with the literature[1,24] and the previously published results. This testifies a region of restricted mobility and higher crosslinking density close to the interface, favored by rubber-curing agent diffusion and/or chemical interactions with RFL. The thickness of this region is around 15 µm.

The rubber moduli gradient should favor an efficient stress distribution under fatigue loading and then better interfacial strength as it was demonstrated for glass/epoxy composites.[39,40] Interestingly, E_r exponentially increases inside the RFL to reach the polyamide value (≈4 GPa).

After 44 million cycles, interfacial region is reduced and both RFL and interfacial material have reached higher moduli than polyamide [Figure 15(b)]. Such behavior could explain the appearance of RFL/textile delaminations and debondings, respectively, highlighting the previous peeling results and SEM observations.

Interestingly, in the RFL layer, moduli profile is not following its initial exponential increase from rubber value to polyamide one. On the contrary, higher indentation moduli reached close to the rubber interface. This potentially confirms that fatigue loading, causing interfacial shear stress concentration and local heating at the RFL/rubber interface, would favor hardening by thermal ageing and/or interdiffusion of chemicals.

Composites without RFL. For composites without RFL, before fatigue loading [Figure 15(c)], almost the same increase of indentation modulus is observed, close to the interface. This fact could indicate that higher moduli in this area are preferentially caused by chemical diffusions from the bulk rubber than from textile or RFL.

After fatigue loading [Figure 15(d)], bulk rubber and interfacial material moduli have also increased for the composite without RFL. However, they never overpass 4 GPa, the fibers modulus.

To sum up, comparing the two types of composites before fatigue loading, higher rubber moduli are measured close to the textile/rubber interface regardless of the presence of RFL. Such phenomenon is then mainly attributed to rubber curative

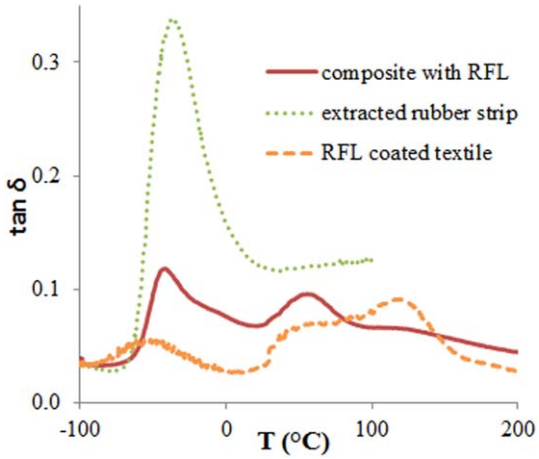

Figure 16. DMA responses of references for composite damping peak attribution. [Color figure can be viewed in the online issue, which is available at wileyonlinelibrary.com.]

diffusion during composite molding. After fatigue loading, interfacial properties of the composite without RFL are few impacted. On the contrary, fatigue loading of composite with RFL drives to strong RFL and interfacial material hardenings, resulting in local Young's moduli higher than polyamide one. This potentially explains the appearance of RFL/textile debondings.

Having in mind the singularities of interfacial Young's moduli, DMA is carried out on composites with or without RFL to extract interphase contribution to global damping. It will be then followed with fatigue.

Interfacial Properties Probed by DMA Temperature Sweeps

First, DMA experiments are carried out on RFL-coated textile and on bulk rubber thin layers extracted from composites before fatigue tests with a cutting tool (15 mm × 15 mm × 0.5 mm). This allows attributing the different damping transitions of the DMA response of composites with RFL, before fatigue loading (Figure 16).

As a result, tan δ peak at −42°C is attributed to glass transitions of the rubber matrix. The peaks at ∼60 and 120°C are attributed to polyamide glass transitions and the one at −50°C to its β transition.

When DMA response of initial composites with RFL is compared to fatigue tested ones for 44 million cycles, some differences are noticed [Figure 17(a)]. First, an increase of the global storage modulus all along the temperature range. This is contradictory with the literature assessing that a weaker interface leads to a smaller composite modulus.[25,41–43] However, such assessments are mainly obtained from the comparison between composites with different adhesive formulations but with the same matrix and reinforcements. In our case, the last two can also evolve in fatigue as it was showed by nanoindentation. Indeed, bulk rubber Young's modulus was six times higher after 44 millions of fatigue loading (Figure 14).

When analyzing tan δ evolutions, a shoulder above the rubber glass transition, at around −20°C, is detected for the initial composite with RFL [Figure 17(a)]. Such shoulder is also slightly detected on an initial composite without RFL [Figure 17(b)] and hence it cannot be attributed to the RFL latex phase but more certainly to the rubber. However, extracted rubber strip (Figure 16) did not show such a shoulder. It could then testify a region of restricted mobility of the rubber phase close to the textile: an interphase. Such phenomenon has already been pointed out in composite as glass or carbon fiber-reinforced epoxies or vinyl esters.[44,45]

As this shoulder has completely disappeared after 44 millions of fatigue cycles, it could indicate damages or at least structural changes at the RFL/rubber interface.

To quantify those changes, composite damping intensity evolutions at −43°C are followed with fatigue. However, as they integrate both interfacial and bulk rubber contributions, the last ones are evaluated by carrying out DMA temperature sweeps on composites' bulk rubber strips, extracted with a cutting tool, at different fatigue loading times (Figure 18). The results highlight a linear decrease with fatigue in the damping intensity of bulk rubber.

Then, to quantify interfacial changes, taking into account bulk rubber properties evolutions, the method introduced by Zorowski and Murayama is used.[26,27] It allows the calculation of the energy dissipation at the interface owing to poor adhesion, tan δ_{int}:

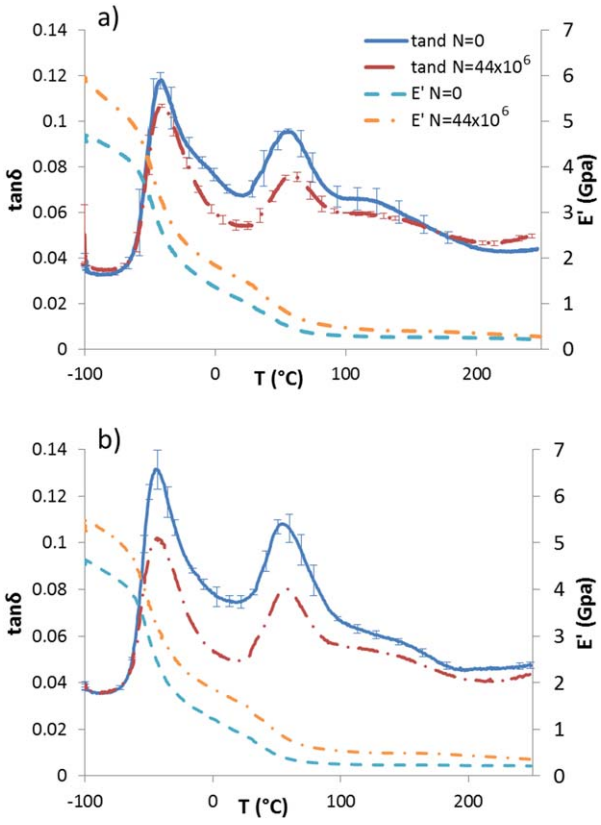

Figure 17. Fatigue impact on storage modulus and damping for composites (a) with RFL and (b) without RFL. [Color figure can be viewed in the online issue, which is available at wileyonlinelibrary.com.]

$$\tan\delta_{int} = \tan\delta_c - \tan\delta_0 \quad (7)$$

$$\tan\delta_0 = \frac{\tan\delta_f E_f v_f + \tan\delta_m E_m v_m}{E_f v_f + E_m v_m} \quad (8)$$

where tan δ_c is the damping of the composite measured by DMA, tan δ_0, the damping of a model composite with perfect adhesion, E is the storage part of dynamic response, v is the volume fraction, and subscript f or m refer to the fibers (cords) or the matrix (rubber).

Calculations are made from DMA curves of RFL-coated cord, RFL-uncoated cord, extracted rubber strips, and composites at maximum rubber damping, that is $-42°C$ ($v_f = (N\pi 0.5^2 \times 30)/(30 \times 15 \times 1.7) = [0.33; 0.4]$, $v_m = 1 - v_f = [0.6; 0.67]$ with N the number of cords per composite).

Before fatigue loading, composites with RFL show a lower tan δ_{int} value than composites without RFL. Based on Murayama's results, such lower value could be correlated with their better peeling strength, the interface is being less dissipative through frictional phenomena.[46]

However, until 15 million cycles, both composites show a drop in tan δ_{int}, linked with a drop in peeling strength, and hence in contradiction with Murayama's assessments. However, he did not consider the interface as a three-dimensional area which is the case of cord–rubber composites as proved by nanoindentation. Then, more than frictional dissipations, tan δ_{int} could also

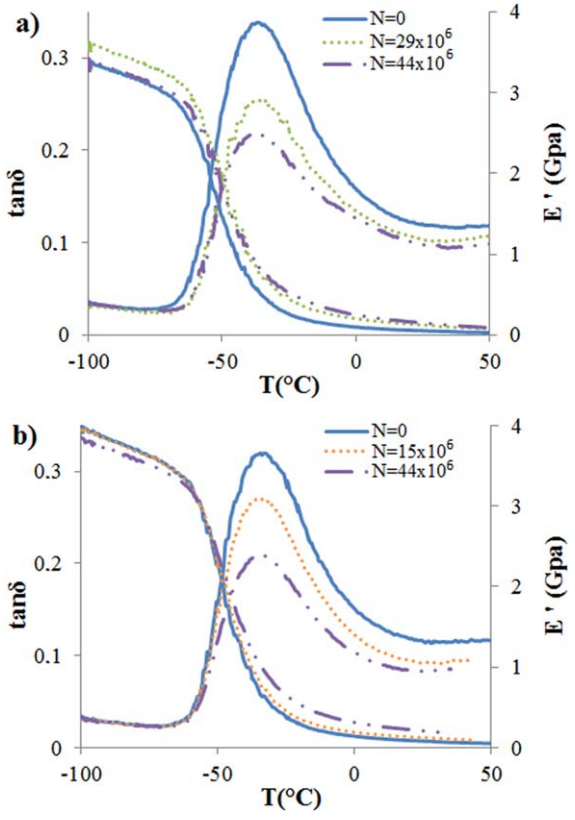

Figure 18. Fatigue impact on tan δ of extracted rubber strips from composites (a) with RFL and (b) without RFL. [Color figure can be viewed in the online issue, which is available at wileyonlinelibrary.com.]

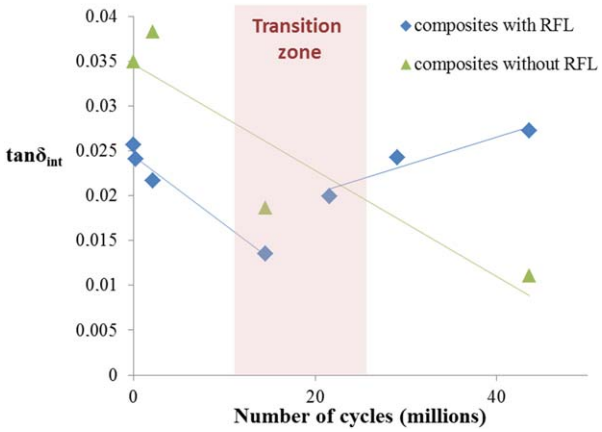

Figure 19. Interfacial damping versus fatigue loading. [Color figure can be viewed in the online issue, which is available at wileyonlinelibrary.com.]

involve viscoelastic properties of the interphase itself. Consequently, the strong increase of interfacial rubber Young's modulus in fatigue, revealed by nanoindentation, could lead to a decrease of interphase damping, compensating the energy dissipation owing to poor adhesion.

Taking a closer look at tan δ_{int}, it decreases for both composites until 20 million cycles, in good correlation with a decrease of the viscoelastic properties of the interphase caused by a local hardening. However, for composites with RFL, because of RFL/rubber interfacial delamination, more parameters than only interphase viscoelasticity could contribute to tan δ_{int} value[47] as: the percentage of bounded regions at the interface, i.e. the volume fraction of interphase really loaded, and frictional damping, owing to the slip in the unbounded interfacial regions.

Interestingly, a sudden jump of tan δ_{int} is observed above 15 million cycles for composites with RFL. Even if this phenomenon is not completely explained yet, it is worth to notice that it happens in the "peeling transition zone" previously introduced, meaning that it could be link with the appearance of fiber/RFL debondings.

CONCLUSIONS

Peeling tests, SEM–EDX observations, nanoindentation tests, and DMA allowed probing structural or mechanical properties of the interphase of polyamide-reinforced rubber composites.

These combined techniques have highlighted two main damages mechanisms for the fatigue-loaded composites with RFL: propagation of pre-existing fibrillar microcracks at the rubber/RFL interface and adhesive debondings between textile microfilaments and RFL.

At the RFL/rubber interface, the microcrack propagation mechanism evolves in three stages, reaching 60% delamination after 44 million cycles. The first stage of RFL/rubber delamination is correlated with a decrease of peeling resistance and of tan δ_{int}, calculated from DMA temperature sweeps. Such mechanical

property degradations are linked, at a local scale, to a strong increase of Young's moduli of both RFL and closest rubber. This hardening is attributed to chemical diffusions, as rubber-curing agents, but also thermomechanical ageing caused by high local stresses.

Concerning adhesive debondings at the RFL/textile interface, they occur only after approximately 15 million fatigue loading cycles. This phenomenon is highlighted with a change of failure surface through peeling tests. It is correlated with a linear decrease of the peeling resistance, RFL, and interfacial material moduli reaching polyamide one, a sudden jump of RFL/fiber debondings observed by SEM and a slowering of the first RFL/rubber crack propagation mechanism.

As for composites without RFL, they show a lower peeling strength at the initial stage. However, their interfacial properties are less impacted by fatigue loading and such composites never show the failure mode of textile pull out on the edge. This could be explained by a better anchoring of rubber as it is observed by SEM. Nanoindentation experiments also demonstrate that moduli of the corresponding interfacial material evolve in a better way in fatigue, to give a continuous gradient between bulk rubber and polyamide fiber values. However, such composite without RFL cannot fulfill other industrial requirements and cannot be the solution for life expectancy improvements.

Then, to improve fatigue resistance of the composites with RFL, one way could be to explain and reduce RFL hardening through thermomechanical loading. This should allow postponing the appearance of the RFL/textile debondings.

ACKNOWLEDGMENTS

The authors thank "Le département des microscopies" of the University of Tours for their technical support on SEM–EDX observations.

REFERENCES

1. Wennekes, W. B. Adhesion of RFL-Treated Cords to Rubber: New Insights into Interfacial Phenomena; University of Twente, The Netherlands, **2008**; p 1.
2. Durairaj, R. B. Resorcinol: Chemistry, Technology and Applications; Springer, Berlin, Heidelberg, **2005**; p 1.
3. Darwish, N. A.; El-Wakil, A. A.; Abou-Kandil, A. I. *Int. J. Adhes. Adhes.* **2009**, *29*, 745.
4. Shmurak, I.; Uzina, R. *Polym. Sci. U.S.S.R.* **1966**, *8*, 2280.
5. Iyengar, Y. *J. Appl. Polym. Sci.* **1969**, *13*, 353.
6. Jamshidi, M.; Afshar, F.; Mohammadi, N.; Pourmahdian, S. *Appl. Surf. Sci.* **2005**, *249*, 208.
7. Job, L.; Joseph, R. *J. Appl. Polym. Sci.* **1999**, *71*, 1197.
8. Darwish, N. A.; Shehata, A. B.; Lawandy, S. N.; Abou-Kandil, A. I. *J. Appl. Polym. Sci.* **1999**, *74*, 762.
9. Koc, S. *Appl. Surf. Sci.* **2008**, *254*, 7049.
10. Aytac, A.; Yilmaz, B.; Deniz, V. *Fibers Polym.* **2009**, *10*, 221.
11. Fulton, W. *Appl. Surf. Sci.* **2004**, *221*, 69.
12. Luo, S. Surface Modification of Textile Fibers and Cords by Polymeric Matrices; University of Cincinnati, **2002**.
13. Ashirgade, A. A. Mechanistic study of the rubber-brass adhesion interphase, University of Cincinnati, USA, **2010**.
14. Jamshidi, M.; Afshar, F.; Shamayeli, B. *J. Appl. Polym. Sci.* **2006**, *101*, 2488.
15. Krump, H.; Hudec, I.; Jasso, M.; Dayss, E.; Luyt, A. *Appl. Surf. Sci.* **2006**, *252*, 4264.
16. Langevin, P. P.; Payne, R. J.; Shephard, C. S. *Rubber Chem. Technol.* **1974**, *47*, 171.
17. Wagner, M. P.; Hewitt, N. L. *Rubber Chem. Technol.* **1979**, *52*, 805.
18. Abou-Kandil, A. I.; Awad, A.; Darwish, N.; Shehata, A. B.; Saleh, B. K. *Int. J. Adhes. Adhes.* **2013**, *44*, 26.
19. Shi, X.; Ma, M.; Lian, C.; Zhu, D. *Polym. Test.* **2013**, *32*, 1145.
20. Rao, S.; Daniel, I. M.; Gdoutos, E. E. *Appl. Compos. Mater.* **2004**, *11*, 353.
21. Ku, B. H.; Liu, D. S.; Lee, B. L. *Rubber Chem. Technol.* **1998**, *71*, 889.
22. Lake, G. J. *Rubber Chem. Technol.* **2001**, *74*, 509.
23. Liu, Y.; Wan, Z.; Tian, Z.; Du, X.; Jiang, J.; Yao, M. *Tire Sci. Technol.* **1999**, *27*, 48.
24. Stevens, C. A. In Polymer Bonding 2004: 1st International Conference Focussing on the Bonding of Rubbers and Plastics to Various Substrates; Rapra Technology Limited: Munich, **2004**, p 67.
25. Ibarra, L.; Chamorro, C. *Polym. Compos.* **1989**, *10*, 256.
26. Zorowski, C. F.; Murayama, T. in Proceedings of the 1st International Conference on Mechanical Behaviour of Materials, vol 5, Society of Material Science, Kyoto, **1972**, p 28.
27. Murayama, T.; Lawton, E. L. *J. Appl. Polym. Sci.* **1973**, *17*, 669.
28. Afaghi-Khatibi, A.; Mai, Y.-W. *Compos. Part A: Appl. Sci. Manuf.* **2002**, *33*, 1585.
29. Oliver, W. C.; Pharr, G. M. *J. Mater. Res.* **1992**, *7*, 1564.
30. Bielinski, D. M. *KGK Kautschuk, Gummi, Kunststoffe* **2009**, *62*, 50.
31. Jeol, S.; Badel, T. Stabilised polyamide composition. WO2012140099A1, **2012**.
32. Jagota, A.; Bennison, S. J. *Integr. Comp. Biol.* **2002**, *42*, 1140.
33. Oyen, M. L. *J. Mater. Res.* **2005**, *20*, 2094.
34. VanLandingham, M. R.; Villarrubia, J. S.; Guthrie, W. F.; Meyers, G. F. *Macromol. Symp.* **2001**, *167*, 15.
35. Deuschle, J. K.; Deuschle, H. M.; Enders, S.; Artz, E. *J. Mater. Res.* **2009**, *24*, 736.
36. Lee, G.; Kang, S.-K.; Kwon, D. *Mater. Sci. Eng. A. Struct. Mater.* **2008**, *496*, 494.
37. Wootthikanokkhan, J.; Burford, R. P.; Chaplin, R. P. *J. Appl. Polym. Sci.* **1998**, *67*, 1277.

38. Lake, G. J.; Thomas, A. G. *Proc. R. Soc. A Math. Phys. Eng. Sci.* **1967**, *300*, 108.
39. Gao, S. *Compos. Part A: Appl. Sci. Manuf.* **2002**, *33*, 559.
40. Hodzic, A. *Micron.* **2001**, *32*, 765.
41. Rajeev, R. S.; Bhowmick, A. K.; De, S. K.; Kao, G. J. P.; Bandyopadhyay, S. *Polym. Compos.* **2002**, *23*, 574.
42. Jacob, M.; Francis, B.; Thomas, S. *Polym. Compos.* **2006**, *27*, 671.
43. Rajeev, R. S.; Bhowmick, A. K.; Bandyopadhyay, S. *J. Appl. Polym. Sci.* **2003**, *90*, 544.
44. Thomason, J. L. *Polym. Compos.* **1990**, *11*, 105.
45. Verghese, K. E.; Jensen, R.; Lesko, J.; Ward, T. *Polymer* **2001**, *42*, 1633.
46. Murayama, T. *J. Appl. Polym. Sci.* **1979**, *24*, 1413.
47. Chandra, R.; Singh, S. P.; Gupta, K. *Compos. Struct.* **1999**, *46*, 41.